Effect of spatial heterogeneity on level of rejuvenation in $Ni_{80}P_{20}$ metallic glass

Tzu-Chia Chen[1], Mahyuddin KM Nasution[2,†], Abdullah Hasan Jabbar[3,‡], Sarah Jawad Shoja[4], Waluyo Adi Siswanto[5], Sigiet Haryo Pranoto[6], Dmitry Bokov[7], Rustem Magizov[8], Yasser Fakri Mustafa[9], A. Surendar[10], Rustem Zalilov[11], Alexandr Sviderskiy[12], Alla Vorobeva[13], Dmitry Vorobyev[13], and Ahmed Alkhayyat[14]

[1] *Dhurakij Pundit University, Bangkok* 10210, *Thailand*
[2] *Data Science and Computational Intelligence Research Group, Universitas Sumatera Utara, Medan, Indonesia*
[3] *Optical Department, College of Health and Medical Technology, Sawa University, Ministry of Higher Education and Scientific Research, Al-Muthanaa, Samawah, Iraq*
[4] *College of Health & Medical Technology, Al-Ayen University, Iraq*
[5] *Faculty of Engineering, Universitas Muhammadiyah Surakarta, Jawa Tengah* 57102, *Indonesia*
[6] *Department of Mechanical Engineering, Faculty of Science and Technology, Universitas Muhammadiyah Kalimantan Timur, Samarinda* 75124, *Indonesia*
[7] *Institute of Pharmacy, Sechenov First Moscow State Medical University,* 8 *Trubetskaya St., Bldg.* 2, *Moscow* 119991, *Russia*
[8] *Kazan Federal University, Kazan, Russia*
[9] *Department of Pharmaceutical Chemistry, College of Pharmacy, University of Mosul, Mosul*-41001, *Iraq*
[10] *Department of Pharmacology, Saveetha Dental College and Hospital, Saveetha Institute of Medical and Technical Sciences, Chennai, India*
[11] *Nosov Magnitogorsk State Technical University, Magnitogorsk, Russia*
[12] *Innovative University of Eurasia, Pavlodar, Republic of Kazakhstan*
[13] *K. G. Razumovsky Moscow State University of Technologies and Management (The First Cossack University), Moscow* 109004, *Russia*
[14] *College of Technical Engineering, The Islamic University, Najaf, Iraq*

(Received 27 December 2021; revised manuscript received 16 March 2022; accepted manuscript online 28 March 2022)

Understanding the relation between spatial heterogeneity and structural rejuvenation is one of the hottest topics in the field of metallic glasses (MGs). In this work, molecular dynamics (MD) simulation is implemented to discover the effects of initial spatial heterogeneity on the level of rejuvenation in the $Ni_{80}P_{20}$MGs. For this purpose, the samples are prepared with cooling rates of 10^{10} K/s–10^{12} K/s to make glassy alloys with different atomic configurations. Firstly, it is found that the increase in the cooling rate leads the Gaussian-type shear modulus distribution to widen, indicating the aggregations in both elastically soft and hard regions. After the primary evaluations, the elastostatic loading is also used to transform structural rejuvenation into the atomic configurations. The results indicate that the sample with intermediate structural heterogeneity prepared with 10^{11} K/s exhibits the maximum structural rejuvenation which is due to the fact that the atomic configuration in an intermediate structure contains more potential sites for generating the maximum atomic rearrangement and loosely packed regions under an external excitation. The features of atomic rearrangement and structural changes under the rejuvenation process are discussed in detail.

Keywords: metallic glasses, mechanical properties, molecular dynamics simulation, disordered solids

PACS: 64.70.pe, 78.55.Qr **DOI:** 10.1088/1674-1056/ac615e

1. Introduction

Owing to their individual amorphous structures, metallic glasses (MGs) possess superior mechanical properties.[1–3] However, this unique feature comes at the expense of poor tensile ductility with severe localization of plasticity.[4–6] Rejuvenation process is one of the main methods of improving the ductility behavior of MGs under an external loading.[7–10] In a rejuvenated structure, the atomic configuration becomes excited somehow to generate the loosely packed regions like free volumes within the glassy matrix.[11,12] In recent years, several techniques have been proposed to rejuvenate the glassy alloys; however, it has been uncovered that there is a saturated state or an optimized level for the structural excitation.[13–15]

To provide some examples, Wakeda and Saida[16] simulated the thermal rejuvenation process of CuZr system by using molecular dynamics (MD) to find the mechanism of structural rearrangements. It was revealed that the structural rejuvenation, correlated with the decrease of ordered configurations, can also generates newly ordered local structures. This was identified as a key reason for the saturation of rejuvenation in the MGs. In another work, Shayakhmetov *et al.*[17] showed that an optimized state exists for the rejuvenation under the mechanical attrition treatment, which may be due to the saturation of anelastic strain energy in the body of glassy material. Using the synchrotron x-ray diffraction, it was also found that in highly deformed regions under the highpressure torsion the local mean atomic volume is increased up to about 0.75%, thus

†Corresponding author. E-mail: mahyuddin.nasution198@gmail.com
‡Corresponding author. E-mail: abdullah.hasan.j@sawa-un.edu.iq

achieving a saturated rejuvenated structure.[18] Under the elastostatic loading, it was revealed that a saturated state happens in the structural rejuvenation, which is due to the mutation of positional atomic rearrangements in the alloying system.[19,20] Implementing MD simulation, Li *et al.*[21] demonstrated that the atomic packing density transitions within different regions of glassy structure are responsible for accumulated rejuvenation in the cyclic-loaded MGs. Wang and Yang[22] simulated different chemical compositions of CuZr alloys under the cyclic loading and found that the optimized structural rejuvenation strongly depends on the fraction of ordered coordination polyhedron. Kim *et al.*[23] unveiled that the population of flow units in a thermal rejuvenation is chiefly influenced by the final cooling rate rather than the quenching temperature. Kang *et al.*[24] also confirmed that an intermediate structural state is required for optimizing the structural excitation through the cryogenic cycling process. Utz *et al.*[25] produced the binary MGs at different cooling rates and evaluated the structural rejuvenation based on the potential energy landscape. They reported that the lower the initial energy of MG (slow cooling rate) the higher the internal stress in a rejuvenation process is, where the elastic regime transforms into the plastic state. Using elastostatic loading, Zhang *et al.*[26] proposed a model based on the de-mixing tendency, in which a competitive relationship between activation enthalpy and activation entropy explains the stress threshold in the relaxation/rejuvenation of MGs. Jiang *et al.*[27] produced the CuZr MGs at different cooling rates for obtaining the glassy structures with a wide range of potential energy. They found that the rejuvenation process in a sample with low potential energy leads more cavities to be created in the microstructure; however, a saturated state was detected between the population of cavities and initial potential energy. In another study, it was unveiled that the generation and distribution of free volumes under the shot peening process is mainly dependent on the initial state of relaxation in the MGs.[28]

As mentioned above, several studies have been performed experimentally and numerically, showing that there exist an optimized or saturated state in the structural rejuvenation of MGs. However, the reasons for inducing optimized state are still under debate. It is suggested that the initial structural heterogeneity is a crucial parameter for maximizing the level of rejuvenation in the glassy structures. Hence, the manipulation of atomic configuration in the initial state significantly affects the intensification of rejuvenation in the MGs. To unveil the mechanism of optimum rejuvenation in the MGs, the $Ni_{80}P_{20}$ glassy alloy was modeled with three different cooling rates, *i.e.*, 10^{10} K/s, 10^{11} K/s, and 10^{12} K/s, leading to a wide range of structural heterogeneity in the system. Afterward, an identical elastostatic loading process is carried out for each sample to show how many changes take place in the level of rejuvenation in each state. The rate of rejuvenation increment in the treated sample is determined through a relative study in each state. The outcome of this work clearly shows the significance of heterogeneity manipulation for achieving an optimum rejuvenation state.

2. Computational method

In this study, the molecular dynamics (MD) approach was considered for modeling the behavior of MG. For this purpose, the MD calculations were conducted by the embedded-atom method (EAM) for an Ni–P alloying system presented by Sheng *et al.*[29] It should be noted that the simulations were performed through large-scale atomic/molecular massively parallel simulator (LAMMPS) code at zero external pressure in the isothermal isobaric ensemble (NPT).[30] The $Ni_{80}P_{20}$ alloying system with 4.5×10^4 atoms was modeled; while the periodic boundary conditions were considered in all the directions. The temperature of system was controlled by the Nose-Hoover thermostat[31] and the calculations were performed in integration time steps of 1 fs. To make the primary atomic configuration with $Ni_{80}P_{20}$ composition, the P atoms were randomly inserted into the cell of Ni with face centered cubic lattice. The system was then melted and equilibrated at a temperature of 2000 K for 0.3 ns and 2 ns, separately. The quenching processes with cooling rates of 10^{10} K/s, 10^{11} K/s, and 10^{12} K/s were performed to make the solid atomic configurations at 300 K. Hereafter, a replication process along with a relaxation treatment were carried out to enlarge the atomic box. It should be noted that the quenched samples under the cooling rates of 10^{10} K/s, 10^{11} K/s, and 10^{12} K/s were denoted as S10, S20, and S30 in the following sections. To picture the spatial heterogeneity of MGs, the atomic computational tomography (ACT) was employed by considering the elastic properties of structure. In this technique, a unique parameter was determined to explain the type and fluctuations of atomic pairs in a certain spherical volume and characterize the shear modulus of nanoscale regions in the MG structure. This technique, described in Ref. [21], established a meaningful relation between the packing density and elastic features of the alloying system.

After preparing the sample, the elastostatic loading process under at temperature of 300 K was implemented. The normal stress was employed along the z direction; while the loading was continued for 6000 τ ($\tau = 2.09 \times 10^{-11}$ s) under 90% of yield strength. It should be noted that there does not exist any pressure along the x direction nor the y direction and the system was affected only by a static normal stress along the z direction.[32] After the loading process, the normal stress decreased to that of the reference state ($P = 0$) and then relaxed for 1 ns. In the elastostatic loading process, all the parameters including the dimension, potential energy and stress components were recorded for subsequent evaluations. The states of

elastostatically loaded samples S10, S20, and S30 were denoted as S11, S21, and S31, respectively. It should be noted that the simulation was performed three times for each state to ensure the reliability of data acquisition. The schematic diagram of sample preparation and rejuvenation process is given in Fig. 1.

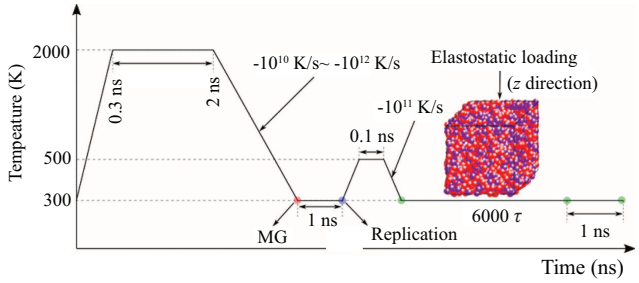

Fig. 1. Schematic diagram of sample preparation and elastostalic loading process for optimizing the structural rejuvenation in MGs.

3. Results and discussion

3.1. Identification of spatial heterogeneity

The first step is to find out the effects of cooling rates on the nanoscale spatial heterogeneity in the prepared alloys. For this purpose, a fluctuation method is used to evaluate the isothermal stiffness coefficient at 300 K[33]

$$C^{\mathrm{T}}_{ijkl} = C^{\mathrm{I}}_{ijkl} + C^{\mathrm{II}}_{ijkl} + C^{\mathrm{III}}_{ijkl}. \tag{1}$$

In this equation, the Born, kinetic, and contribution terms are marked by the superscripts I, II, and III. As depicted in Ref. [13], the mean shear modulus (G) can be calculated from $G = (C_{44} + C_{55} + C_{66})/3$, in which the G term results from the combination of three terms mentioned in Eq. (1). Using this approach, it is possible to characterize the local shear elasticity from angstrom-scale to the larger-scale spatial region in the MG.

As mentioned in Section 2, the samples are prepared with the relaxation times of 0.3 ns and 2 ns at 2000 K. This process is carried out to show how the holding time at high temperature leads the final atomic structure to change. Figure 2 shows the two-dimensional (2D) elastic heterogeneity maps of samples S10, S20, and S30. In general, it is observed that the structural heterogeneity in the sample exposed for 0.3 ns is higher than that in the sample exposed for 2 ns-exposed. It is believed that the holding time at 2000 K provides atomic homogeneity in the liquid state. When the holding time is 2 ns, the atomic homogeneity reaches the maximum state and subsequently, the glassy structure forms a uniform configuration with low structural heterogeneity after quenching treatment. On the other side, in the shorter holding time (0.3 ns), the structural heterogeneity is intensified in the samples. With the structural heterogeneity improved, the efficiency of rejuvenation process will be enhanced in the samples due to the generation of more local stress domains in the atomic system.[19] Hence, in the following, we evaluate the structural variations and the subsequent rejuvenation process based on the samples prepared with the holding time 0.3 ns at 2000 K and later quenching treatment with the cooling rates of 10^{10} K/s, 10^{11} K/s, and 10^{12} K/s, marked as S10, S20, and S30, respectively.

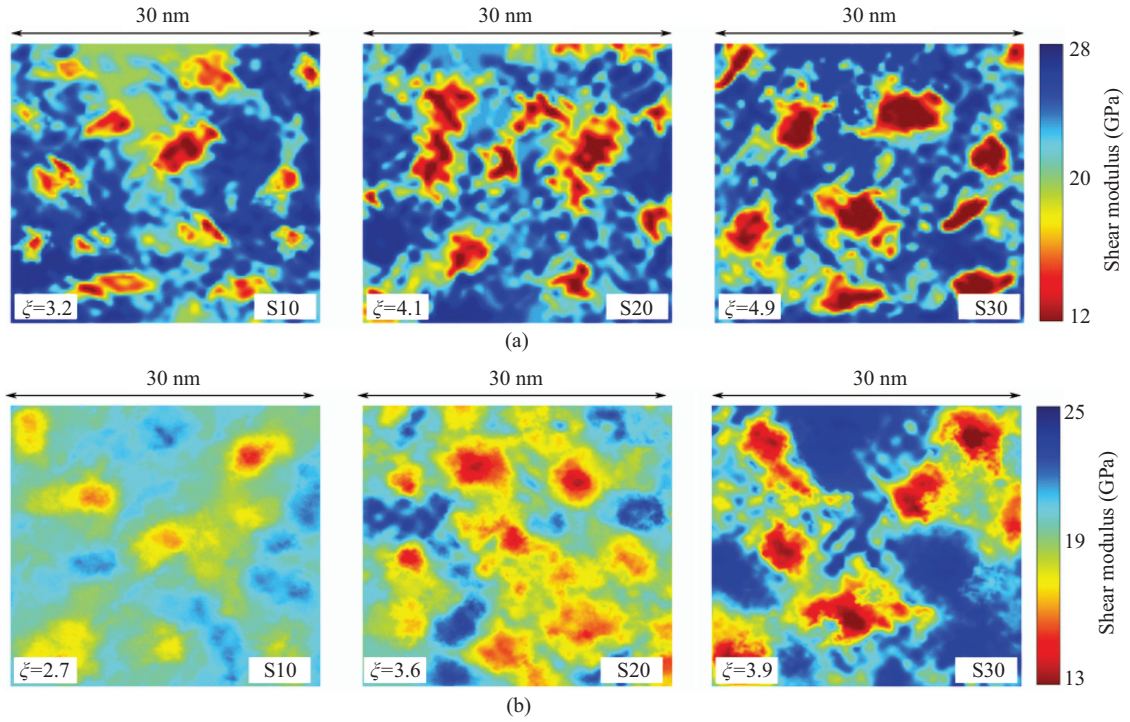

Fig. 2. Snapshots of spatial heterogeneity based on shear modulus for samples exposed for holding time of (a) 0.3 ns and (b) 2 ns at 2000 K and then quenched under the cooling rates of 10^{10} K/s, 10^{11} K/s, and 10^{12} K/s, marked as S10, S20, and S30.

The Gaussian distributions of shear modulus for each sample are given in Fig. 3(a). As observed, the cooling rate plays a significant role in changing shear modulus and spatial heterogeneity in the glassy alloy. With thecooling rate increasing from 10^{10} K/s to 10^{12} K/s, the mean value of Gaussian distribution declines from 22.3 GPa to 19.1 GPa; while the deviation value shows an increasing trend from 3.5 GPa to 6.8 GPa. This means that the increase in cooling rate leads the spatial heterogeneity to be enhanced in the Ni–P MGs. Other experimental researches also showed that the pronounced spatial heterogeneity is accompanied with the increase of Gaussian deviation, which is related to the appearance of local regions with a wide range of elastic properties in the MG structure.[19,34]

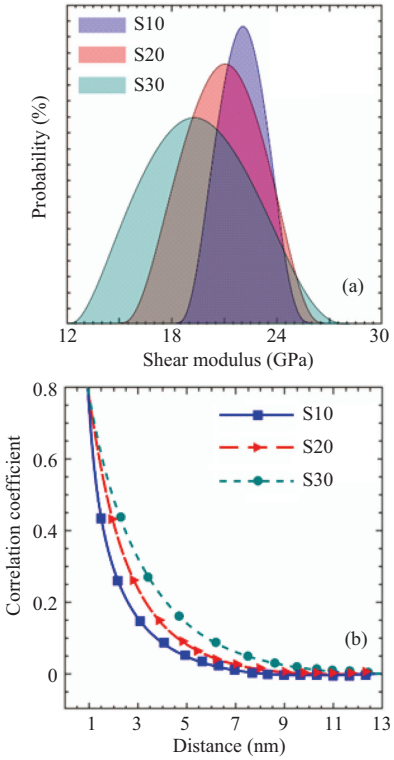

Fig. 3. (a) Gaussian distribution of shear modulus, and (b) correlation coefficient as a function of distance for S10, S20, S30.

To better understand the features of nanoscale heterogeneity in the MGs, the fluctuations of local regions are evaluated by calculating the correlation function of shear modulus, $p(r)$, and achieving the specific correlation length (ξ) through the following equations:[13,35,36]

$$\rho(r) = \frac{\sum_{r_0,r_0+r}(\mu_{r_0} - \bar{\mu})(\mu_{r_0+r} - \bar{\mu})}{\sqrt{\sum_{r_0,r_0+r}(\mu_{r_0} - \bar{\mu})^2}\sqrt{\sum_{r_0,r_0+r}(\mu_{r_0+r} - \bar{\mu})^2}}, \quad (2)$$

$$\rho(r) = \mathrm{e}^{-3r/\xi}, \quad (3)$$

where μ_{r_0} is the shear modulus of a reference position (r_0), and the modulus at the position distance of r is represented by μ_{r_0+r}. Moreover, $\bar{\mu}$ denotes the average of shear modulus. As observed in Figs. 2(a) and 3(b), there is a direct relation between the cooling rates and specific correlation length (ξ). In general, the correlation length determines the scale of fluctuation in the system and introduces the variability of a strongly correlated domain into the structure.[37] Consequently, figure 2(a) clearly shows that the increase of ξ results in the creation of larger clustering areas and the intensification of soft/hard regions in the microstructure. Furthermore, one can see that the "P" function exponentially decays as a function of r value, which is more apparent in systems with lower ξ values. As a result, it is suggested that the higher cooling rates leads to the more pronounced heterogeneity in the glassy structure.

3.2. Elastostatic loading effects

In this subsection, the effects of elastostatic loading on the rejuvenation behavior and atomistic rearrangements of MG samples are investigated. Figure 4(a) shows the tensile stress–strain curves of simulated samples with varying conditions. It is observed that the elastostatic loading effect on the deformation behavior of sample is considerably different. In general, the higher the level of rejuvenation, the more homogeneous the achieved plastic strain deformation is. A failure criterion is also considered to evaluate the plastic strain ratio in the rejuvenated sample. In this work, the failure criterion is the value of plastic strain in the load-displacement curve, in which the main shear band crosses the sample with an average Von Mises strain of 0.5. As observed in Fig. 4(b), the measured values for the homogenous strain ratios of S11/S10, S21/S20, and S31/S30 are 1.24, 1.39, and 1.19, respectively. Here is an example The strain ratio of 1.39 for the S21/S20 shows that the homogenous plastic strain in sample S21 increases by 39% in comparison with that in sample S20. This result is also suggestive of the idea that the primary spatial heterogeneity is responsible for the subsequent effects of elastostatic loading on the deformation behavior of glassy structure. To better characterize the plasticity behavior, the snapshots of shear strain maps for all the samples at a strain of 12% are presented in Fig. 4(c).

It is found that there is a meaningful relation between the correlation length and the deformation mode in the samples. For the sample S10, the deformation behavior is dominated by a single shear band, while the elastostatic loaded state (S11) declines the localized shear events and improves the homogenous plasticity in the alloying system. On the other hand, the rate of the homogenous deformation from sample S20 to sample S21 is more apparent, showing the high capability of this alloying system for the structural rejuvenation. This event is identified in the stress-strain curves, in which a distinctive transition occurs from a stress overshoot (sample S20) to an elastic-nearly plastic deformation (sample S21). Moreover, one can easily see that the local shear events with 45° orientation significantly decline in the structure of the sample S21, indicating the considerable structural rejuvenation under the elastostatic loading. A comparison between samples S30 and

S31 shows that the plasticity improvement is lower than that happens in S20/S21 state. This is due to the fact that the sample S30 with a heterogeneous structure ($\xi = 4.9$ nm) lacks sufficient potential sites for creating new shear events under the elastostatic loading (S31).[13,38] Consequently, the increasing rate of rejuvenation degree in this condition becomes lower than those of other samples. Nevertheless, it is worth mentioning that the treated sample (S31) still exhibits a homogeneous deformation with multiple strain localization paths under the tensile loading.

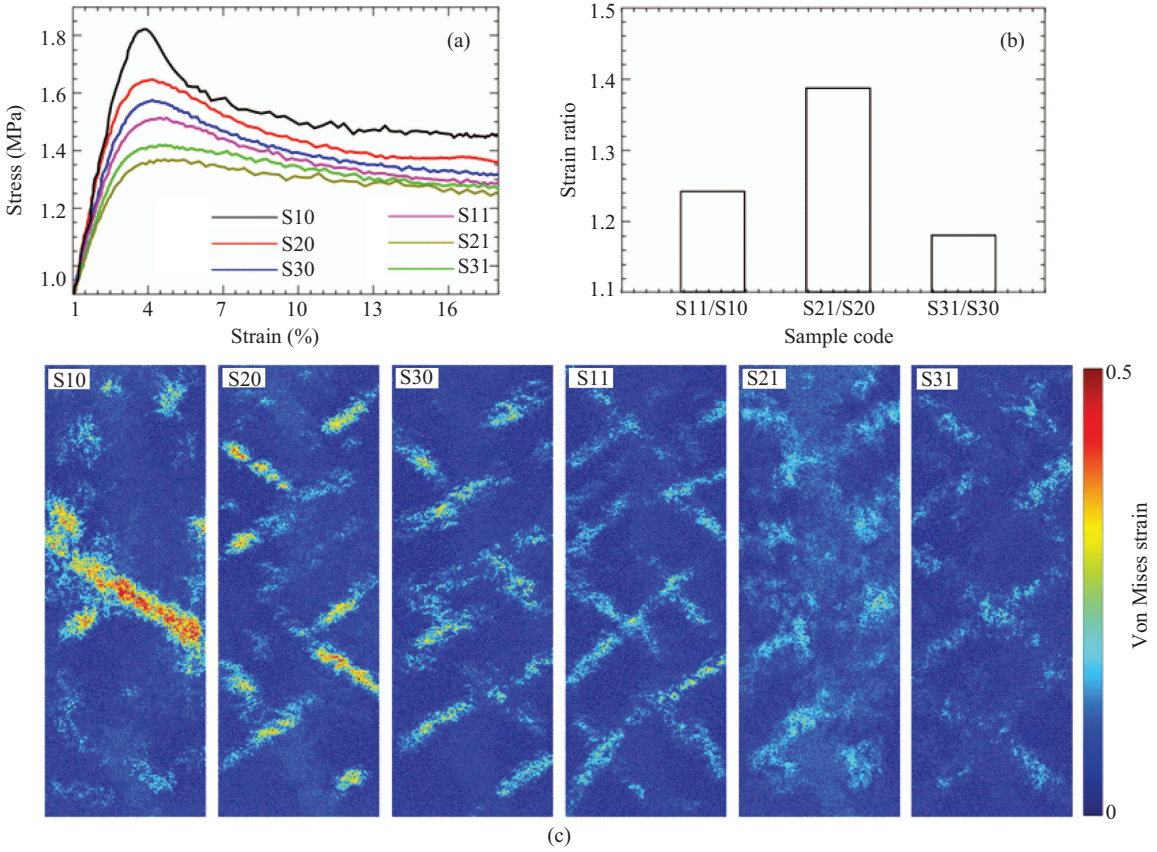

Fig. 4. (a) Tensile stress–strain curves of samples, (b) plastic strain ratios at the failure condition, and (c) snapshots of strain distribution at a strain value of 12% under tensile test.

The assessment of atomic structure by using pair distribution function (PDF) provides significant information regarding the evolution of rejuvenation in the MGs.[39,40] The intensities and positions of peaks in the PDF analysis presents an average density of atoms in a certain distance and reveals the features of short range order and medium range order in the glassy structure. The partial PDF curves can be obtained from the following equation:[41]

$$g_{\alpha\beta}(r) = \frac{N}{4\pi r^2 \rho N_\alpha N_\beta} \sum_{i=0}^{N_\alpha} \sum_{j=0}^{N_\beta} \delta\left(r - |\boldsymbol{r}_{ij}|\right), \tag{4}$$

where N_α and N_β are the numbers of α atoms and β atoms, respectively; ρ is the number density of atoms; $\boldsymbol{r}_{ij}$ is the interatomic distance between two constitutes. Figure 5 shows the partial PDF curves at 250 K for all the samples. There does not exist any peak shift in the Ni–Ni pair nor the Ni–P pairs; however, the P–P pairs shows a slight displacement to the lower r value, indicating the strong interactions of phosphorus atomic pairs after the structural rejuvenation. On the other hand, the peak weakening occurs in a short range order parts of Ni–Ni and Ni–P curves, showing that the structural rejuvenation in $Ni_{80}P_{20}$ system is accompanied with the annihilation of these atomic pairs. In general, the NiP system includes the transition metal–metalloid pairs, in which the solute atoms are surrounded by the solvent ones.[41,42] Moreover, there is a solute–solute avoidance phenomenon, which is manifested in the weak first peak of P–P pairs rather than other atomic pairs. In other words, the first peak of P–P pair is considerably weaker than the other atomic bonds, indicating the rare formation of this kind of pair in the alloying system. Under the rejuvenation process, the strong interactions between metal and metalloid atoms decrease, while P–P pairs show a contraction in the system. This result indicates that the structural rejuvenation tends to annihilate the short range clusters and form more loosely packed regions.[43,44] Although, the curves indicates that the highest variations occur from S20 to S21, the PDF analysis presents a clear picture of rejuvenation increment in none of the samples. Therefore, it is suggested to evaluate the atomic configurations in more detail.

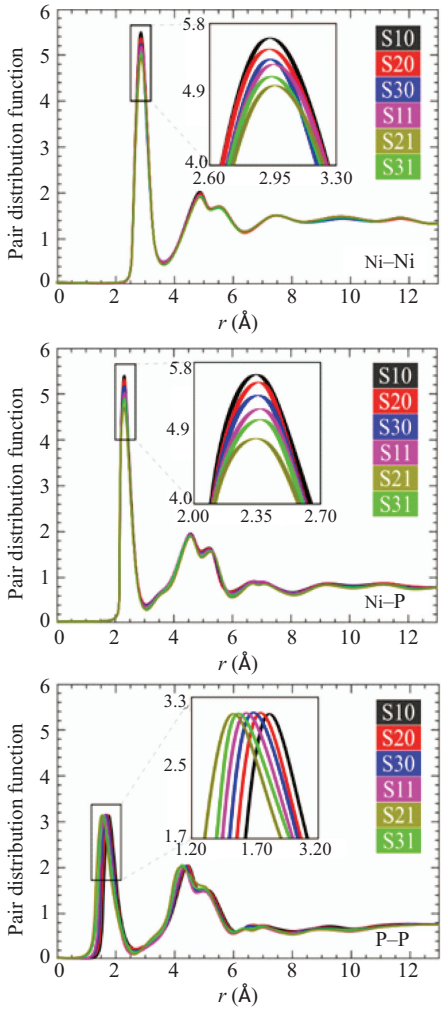

Fig. 5. Partial pair distribution function for all the samples.

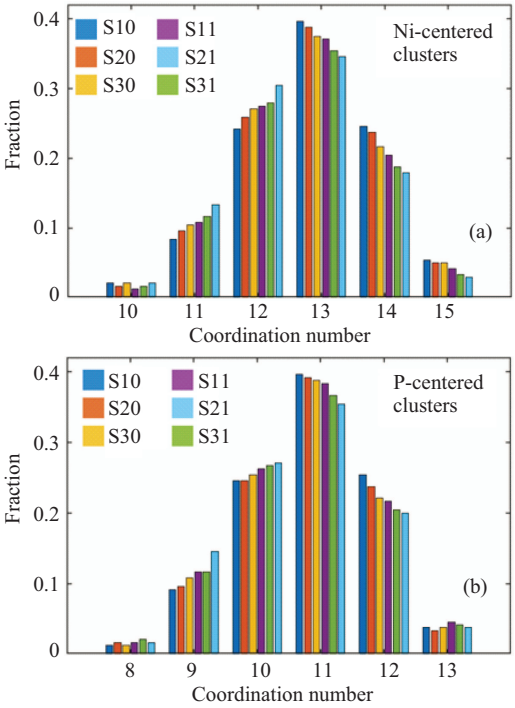

Fig. 6. Fractions of (a) Ni-centered clusters and(b) P-centered clusters as a function coordination number.

The analysis of coordination number (CN) in the first shell of atomic clusters manifests the effects of elastostatic loading on the structural configurations of NiP MG. The distributions of Ni- and P-centered clusters for all the samples are presented in Fig. 6. The figure shows that the mean value of CN in the P-centered clusters is lower than that in the Ni-centered ones, which means that the P-centered clusters have a smaller size with lower number of atoms in the shell. The results also indicate that the structural rejuvenation plays a crucial role in changing the cluster fractions with different CN values. In general, the elastostatic loading leads clusters to decrease sharply with the increase of CN value, implying that the rejuvenated structure prefers to annihilate the large clusters.[45] Moreover, the high CN clusters include weaker atomic bonds, facilitating the destruction of short-range orders and the creation of free volumes in the backbone of MG.[16]

The mean square displacement (MSD) of the atomic constitutes is calculated at 250 K under the elastostatic loading. Figure 7 shows the MSD curves of P and Ni atoms for samples S11, S21, and S31. At first glance, it can seen that a sharp increase of MSD occurs for both Ni and P in all samples. Afterward, the increase rate becomes weakened with the rise in the elastostatic loading. This result is consistent with other studies showing that the structural rejuvenation tends to show a saturated state in the MGs.[20,46] Moreover, the results indicate that the average displacements of atoms in samples are different from each other, so that the sample S21 experiences the maximum atomic displacement during the elastostatic loading but the atomic displacement decreases in the samples S31 and S11, respectively. This event is consistent with the PDF analysis and tensile stress–strain curves, indicating that the increase in the level of rejuvenation from S20 to S21 is sharper than the counterparts in other states. The MSD curves also represent that both P atom and Ni atom exhibit an increasing trend under the elastostatic loading; however, one should note that the P atoms are mainly located in the center of short range scale clusters and rarely tends to be embedded at the shells.[37,43] Hence, their movements in the atomic configuration play an important role in the rejuvenation process of MG. Considering Fig. 7(b), the higher MSD value of P in sample S21 is indicative of more atomic clusters annihilate under the elastostatic loading, which means that S20 sample with intermediate primary spatial heterogeneity (S20) considerably facilitates the introduction of disordering and loosely packed structures under an external excitation. Furthermore, one should note that the smaller atomic size of P element can be a main parameter for the larger MSD. However, it is found that the P atoms show a lower MSD value than the Ni constitutes. In the $Ni_{80}P_{20}$ glassy system, the P atoms act as the solute constitutes, meaning that they are generally located in

the center of SRO clusters forming short-size and stable connection with the Ni atoms.[41] On the other hand, the Ni atoms usually tend to be located at the shells of clusters or distributed in the loosely packed structures. Hence, the Ni constitutes can show a higher atomic movement in the NiP amorphous system. The Voronoi polyhedron analysis is another way to clarify the atomic rearrangements under the elastostatic loading. In general, this method is employed to explain the characteristics of local structures and represent the atomic scale configuration of glassy matrix.[47] The polyhedrons as the basis of atomic structure are distinguished by Voronoi indices such as $\langle n_{i3}, n_{i4}, n_{i5}, n_{i6} \rangle$, in which the n_i determines the i-edged faces of the polyhedrons.

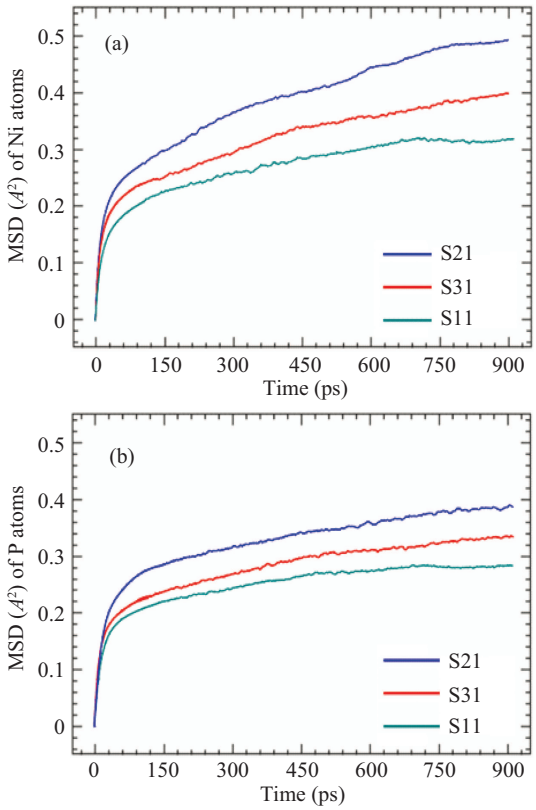

Fig. 7. Mean square displacements (MSDs) of Ni (a) and P (b) atoms under elastostatic loading.

Figure 8(a) represents the ratios of main polyhedrons with 10–13 CN in the samples. In the S21/S20 state, the polyhedron ratios of ⟨0 2 8 2⟩, ⟨0 2 8 1⟩, and ⟨0 1 10 2⟩ all show a sharp increase; while the populations of polyhedrons ⟨0 0 12 0⟩, ⟨0 2 8 0⟩, and ⟨0 3 6 3⟩ decrease under the elastostatic loading. In the S31/30 and S11/S10 states, one can see that the increasing/decreasing trends of polyhedron ratios show slighter features. Moreover, it is observed that the polyhedrons ⟨0 0 12 0⟩ and ⟨0 3 6 3⟩ almost remain unchanged. This result indicates that the sharp rejuvenation in S21/S20 state is associated with the annihilation and generation of specified polyhedrons in the alloying system; while in the less rejuvenated states, *i.e.*, S31/S30 and S11/S10, some polyhedral types resist the reconfigure under the elastostatic loading. It is also significant to understand the reason for creation and annihilation of specified polyhedrons during the elastostatic loading. In general, the polyhedrons ⟨0 2 8 2⟩, ⟨0 2 8 1⟩, and ⟨0 1 10 2⟩ are mostly Ni-centered clusters while, the P-centered ones mainly tend to form polyhedrons ⟨0 0 12 0⟩, ⟨0 2 8 0⟩, and ⟨0 3 6 3⟩. Hence, one can conclude that the rejuvenation process tends to form more Ni-centered clusters in the system. This event is due to the fact that the Ni-centered clusters are energetically less stable than the P-centered ones, resulting in the intensification of disordered structure in the glassy system.[41] Figure 8(b) shows the percentages of free volume in the MG samples. It should be noted that the spatially loosely packed regions with more than −5% deviation from the mean atomic density are considered as the free volumes. According to the results, the increase in cooling rate is responsible for the generation of free volumes in the system. However, one can see that there is an optimal state for the maximum introduction of excess free volumes under the elastostatic loading. In other words, when the free volume content is intermediate in the glassy structure (*i.e.* S20), the conditions for generating more free volumes under the elastostatic become more facilitated (*i.e.*, S21).

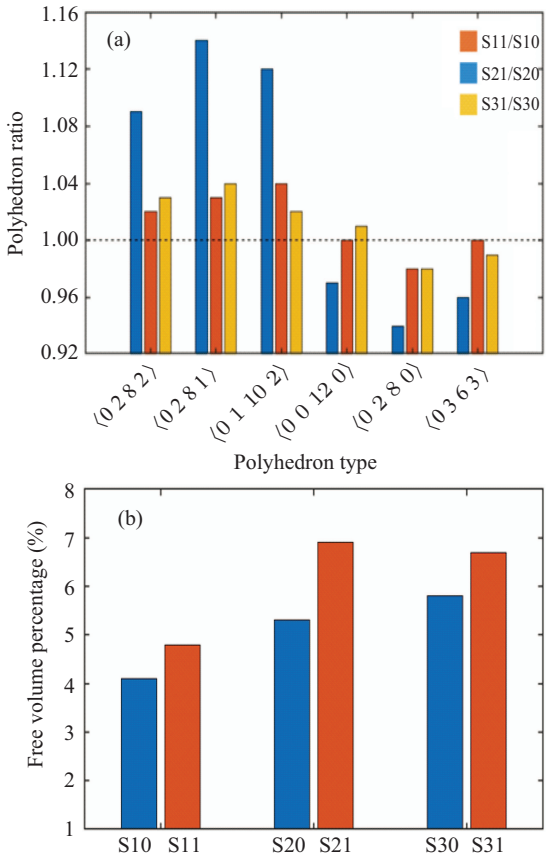

Fig. 8. (a) Polyhedron-type ratios under the elastostatic loading, and (b) percentage of free volume in the samples.

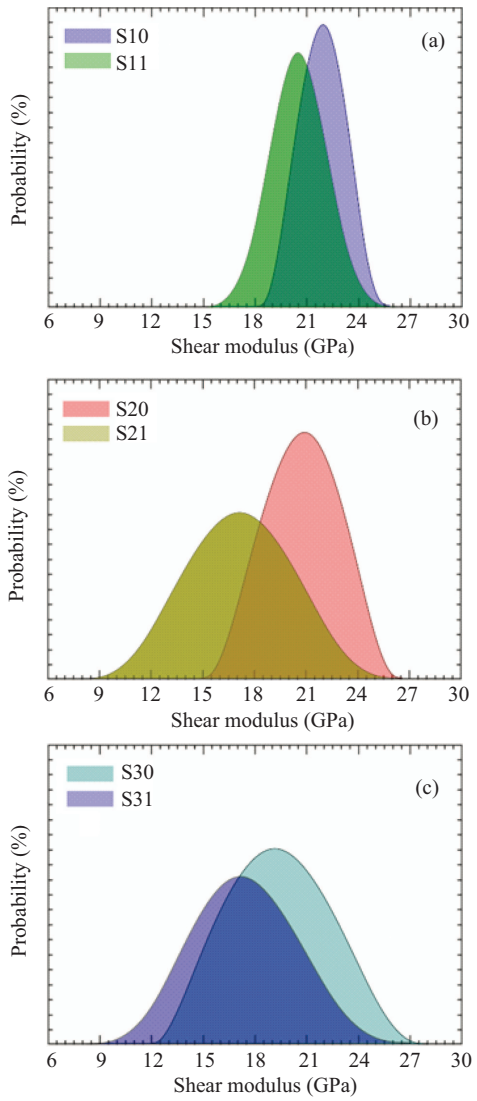

Fig. 9. Gaussian shear modulus distributions of (a) S10 and S11, (b) S20 and S21, and (c) S30 and S31.

On the whole, the results of this work indicate that the initial structural heterogeneity should be in an intermediate state for obtaining the maximum rejuvenation under the elastostatic loading. Other investigations also reported that the achievement of the highest level rejuvenation is correlated with the intermediate structural features of MGs.[24,48] In general, the structural rejuvenation in a glassy structure is associated with the degree of potential sites for the generation of internal stresses, leading to the disordering phenomenon in the system. As given in Figs. 2 and 9, sample S10 mainly includes hard regions with high shear modulus. Moreover, the compact Gaussian distribution of shear modulus shows a homogeneous atomic configuration in this sample. Consequently, the population of potential sites for generation of internal stress is not much enough to induce a significant structural rejuvenation as seen in sample S11. On the other hand, the structural heterogeneity in sample S30 is excessive and the soft regions are dominated in the structure (see Fig. 9). This event results in the damping or relaxation of internal stresses induced by the elastostatic loading. In other words, the glassy structure is too soft to introduce more free volumes in the system (See S31). As a result, the structural rejuvenation cannot exceed a certain value. On the other hand, an intermediate structural heterogeneity (S20) is comprised of more potential sites for generating the internal stress. In other words, the sample S20 is neither extremely soft to relax the applied stress nor extremely hard to inhibit any stress generation in the structure. Hence, the level of structural rejuvenation becomes optimized in this state (S21).

4. Conclusions

In this work, the effects of primary structural heterogeneity on the subsequent structural rejuvenation in the $Ni_{80}P_{20}$ MG are investigated. The main outcomes are as follows.

(i) For the sample preparation, it is unveiled that the cooling rates increasing from 1010 K/s to 1012 K/s gives rise to the intensification of structural heterogeneity and the aggregation in both elastically soft and hard regions.

(ii) The tensile stress-strain curves indicate that the rejuvenation process considerably improves the plasticity in the sample; however, the rate of plastic strain enhancement relies on the primary structural heterogeneity.

(iii) The PDF analysis also indicates that the Ni–Ni and Ni–P pairs are annihilated under the rejuvenation; however, there exists no considerable change in the population of P–P pairs. The detailed evaluation of structure also shows that the Ni–P sample with intermediate structural heterogeneity, *i.e.* prepared with 10^{11} K/s experiences the optimized structural rejuvenation, which is due to the type of atomic configuration in an intermediate structure.

References

[1] Wu Y, Xu B, Sun Y and Guan P 2021 *Chin. Phys. B* **30** 057103
[2] Shi H, Zhou H, Zhou Z, Ding Y, Liu W and Ji J 2022 *J. Non-Cryst. Solids* **576** 121246
[3] Chen T C, Rajiman R, Elveny M, Guerrero J W G, Lawal A I, Dwijendra N K A, Surendar A, Danshina S D and Zhu Y 2021 *Arab. J. Sci. Eng.*
[4] Best J P, Ostergaard H E, Li B, Stolpe M, Yang F, Nomoto K, Hasib M T, Muránsky O, Busch R, Li X and Kruzic J J 2020 *Addit. Manuf.* **36** 101416
[5] Gammer C, Rentenberger C, Beitelschmidt D, Minor A M and Eckert J 2021 *Mater. Des.* **209** 109970
[6] Li D M, Chen L S, Yu P, Ding D and Xia L 2020 *Chin. Phys. Lett.* **37** 86401
[7] Lou Y, Liu X, Yang X, Ge Y, Zhao D, Wang H, Zhang L C and Liu Z 2020 *Intermetallics* **118** 106687
[8] Di S, Wang Q, Yang Y, Liang T, Zhou J, Su L, Yin K, Zeng Q, Sun L and Shen B 2022 *J. Mater. Sci. Technol.* **97** 20
[9] Sun Q, Miskovic D M, Kong H and Ferry M 2021 *Appl. Surf. Sci.* **546** 149048
[10] Dong J, Feng Y H, Huan Y, Yi J, Wang W H, Bai H Y and Sun B A 2020 *Chin. Phys. Lett.* **37** 017103
[11] Das A, Dufresne E M and Maaß R 2020 *Acta Mater.* **196** 723
[12] Zhu Q, Zhang M, Jin X, Yang H, Jia L and Qiao J 2021 *J. Mater. Res.* **36** 2047
[13] Wang N, Ding J, Yan F, Asta M, Ritchie R O and Li L 2018 *npj Comput. Mater.* **4** 19

[14] Guo W, Shao Y, Zhao M, Lü S and Wu S 2020 *J. Alloys Compd.* **819** 152997
[15] Samavatian M, Gholamipour R, Amadeh A A and Mirdamadi S 2019 *J. Non-Cryst. Solids* **506** 39
[16] Wakeda M and Saida J 2019 *Sci. Technol. Adv. Mater.* **20** 632
[17] Shayakhmetov Y, Vorobeva A, Burlankov S, Bogonosov K, Fomin A, Goncharov A, Krasnikov S, Nikolaeva S, Ovsyannikova A and Zekiy A O 2021 *Mater. Res.* **24**
[18] Ebner C, Escher B, Gammer C, Eckert J, Pauly S and Rentenberger C 2018 *Acta Mater.* **160** 147
[19] Samavatian M, Gholamipour R, Amadeh A A and Samavatian V 2020 *Physica B* **595** 412390
[20] Samavatian M, Gholamipour R, Amadeh A A and Mirdamadi S 2019 *Mater. Sci. Eng. A* **753** 218
[21] Li S, Huang P and Wang F 2019 *Comput. Mater. Sci.* **166** 318
[22] Wang P and Yang X 2020 *Comput. Mater. Sci.* **185** 109965
[23] Kim Y H, Lim K R, Lee D W, Choi Y S and Na Y S 2020 *Met. Mater. Int.*
[24] Kang S J, Cao Q P, Liu J, Tang Y, Wang X D, Zhang D X, Ahn I S, Caron A and Jiang J Z 2019 *J. Alloys Compd.* **795** 493
[25] Utz M, Debenedetti P G and Stillinger F H 2000 *Phys. Rev. Lett.* **84** 1471
[26] Zhang M, Wang Y M, Li F X, Jiang S Q, Li M Z and Liu L 2017 *Sci. Rep.* **7** 625
[27] Jiang S, Huang Y and Li M 2019 *Chin. Phys. B* **28** 046103
[28] Concustell A, Mér F O, Surinach S, Baró M D and Greer A L 2009 *Philos. Mag. Lett.* **89** 831
[29] Sheng H W, Ma E and Kramer M J 2012 *JOM* **64** 856
[30] Plimpton S 1995 *J. Comput. Phys.* **117** 1
[31] Martyna G J, Tobias D J and Klein M L 1994 *J. Chem. Phys.* **101** 4177
[32] Priezjev N V 2019 *Comput. Mater. Sci.* **168** 125
[33] Duan G, Lind M L, Demetriou M D, Johnson W L, Goddard III W A, Çağin T and Samwer K 2006 *Appl. Phys. Lett.* **89** 151901
[34] Zhu F, Nguyen H K, Song S X, Aji D P B, Hirata A, Wang H, Nakajima K and Chen M W 2016 *Nat. Commun.* **7** 11516
[35] Kawasaki T, Araki T and Tanaka H 2007 *Phys. Rev. Lett.* **99** 215701
[36] Chiles J P and Delfiner P 2009 *Geostatistics: modeling spatial uncertainty*, Vol. 497 (John Wiley & Sons)
[37] Firouzianbandpey S, Griffiths D V, Ibsen L B and Andersen L V 2014 *Can. Geotech. J.* **51** 844
[38] Kosiba K, Şopu D, Scudino S, Zhang L, Bednarcik J and Pauly S 2019 *Int. J. Plast.* **119** 156
[39] Shang B, Wang W, Greer A L and Guan P 2021 *Acta Mater.* **213** 116952
[40] Kono Y, Higo Y, Gréaux S, Shibazaki Y, Yamada R, Kuwahara H and Kondo N 2021 *High Press. Res.* 1
[41] Hayat F, Yin J, Tabassum A, Hou H, Lan S and Feng T 2020 *Comput. Mater. Sci.* **179** 109681
[42] Priezjev N V 2019 *J. Mater. Res.* **34** 2664
[43] Wang M, Liu H, Li J, Jiang Q, Yang W and Tang C 2020 *J. Non. Cryst. Solids* **535** 119963
[44] Ross P, Kühemann S, Derlet P M, Yu H, Arnold W, Liaw P, Samwer K and Maaß R 2017 *Acta Mater.* **138** 111
[45] Feng S D, Chan K C, Zhao L, Pan S P, Qi L, Wang L M and Liu R P 2018 *Mater. Des.* **158** 248
[46] Tong Y, Dmowski W, Bei H, Yokoyama Y and Egami T 2018 *Acta Mater.* **148** 384
[47] Reddy K V and Pal S 2019 *Comput. Mater. Sci.* **158** 324
[48] Guo W, Yamada R, Saida J, Lü S and Wu S 2018 *Nanoscale Res. Lett.* **13** 398